An Experimental Study on Boundary Layer Transition Detection Over a Pitching Supercritical Airfoil Using Hot-Film Sensors

Arshia Tabrizian[a], Massoud Tatar[a], Mehran Masdari[a,*], Hamidreza Eivazi[a], Mehdi Seddighi[b,*]

[a] *Faculty of New Sciences and Technologies, University of Tehran, Tehran, Iran*
[b] *Associate Prof., Department of Maritime and Mechanical Engineering, Liverpool John Moores University, Liverpool, United Kingdom*

Abstract

In the present work, experimental tests are conducted to study boundary layer transition over a supercritical airfoil undergoing pitch oscillations using hot-film sensors. Tests have been undertaken at an incompressible flow. Three reduced frequencies of oscillations and two mean angles of attack are studied and the influences of those parameters on transition location are discussed. Different algorithms are examined on the hot-film signals to detect the transition point. Results show the formation of a laminar separation bubble near the leading edge and at relatively higher angles of attack which leads to the transition of the boundary layer. However, at lower angles of attack, the amplification of the peaks in voltage signal indicate the emergence of the vortical structures within the boundary layer, introducing a different transition mechanism. Moreover, an increase in reduced frequency leads to a delay in transition onset, postponing it to a higher angle of attack, which widens the hysteresis between the upstroke and downstroke motions. Rising the reduced frequency yields in weakening or omission of vortical disturbances ensuing the removal of spikes in the signals. Of the other important results observed, is faster movement of the relaminarization point in the higher mean angle of attack. Finally, a time-frequency analysis of the hot-film signals is performed to investigate evolution of spectral features of the transition due to the pitching motion. An asymmetry is clearly observed in frequency pattern of the signals far from the bubble zone towards the trailing

*Corresponding author
Email addresses: m.masdari@ut.ac.ir (Mehran Masdari), M.Seddighi@ljmu.ac.uk (Mehdi Seddighi)

edge; this may reflect the difference between the transition and relaminarization physics. Also, various ranges of frequency were obtained for different transition mechanisms.

Keywords: Boundary layer transition, Pitching airfoil, Hot-film measurement, Time-frequency analysis, Laminar separation bubble

---

Nomenclature

Abbreviations

α, AOA	Angle of attack
CTA	Constant temperature anemometer
LSB	Laminar separation bubble
PIV	Particle image velocimetry
Re	Reynolds number($\frac{cU_\infty}{\nu}$)

Symbols

α_0	Mean angle of attack
$\alpha_{\text{amp.}}$	Pitching amplitude
ω	Angular velocity in pitching motion
σ	Standard deviation
φ	Wavelet function
φ^*	Wavelet function complex conjugate
a	Wavelet transform frequency scale
b	Wavelet transform time scale
C	Wavelet coefficient
c	Chord length
C^*	Wavelet coefficient complex conjugate
f	Pitching motion frequency
f_0	Central frequency of wavelet function
k	Reduced frequency ($\frac{\pi f c}{U_\infty}$)
S	Skewness
s	Curved distance from LE
T	Cycle period
U	CTA Output voltage
x	Distance from LE along the chord

1. Introduction

Drag reduction is one of the preliminary considerations in state-of-the-art aerodynamic designs. For the purpose of skin friction reduction, it is of interest to keep a significant portion of the boundary layer over a wing in the laminar state. However, the transition from laminar to turbulence leads to an increase in the total shear stress and the heat exchanged between the wall surface and the flow. Depending on the turbulence level of the freestream flow, the pressure gradient along the laminar boundary layer, the geometrical details, and the surface roughness, there are various possible mechanisms that may take the flow to the transition, e.g. natural, bypass, separated flow, periodic-unsteady, and reverse transitions. In natural transition, where the level of freestream turbulence intensity is less than 1%, transition is typically the result of disturbances growth in the flow, such as Tollmein-Schlichting (T-S) waves or cross-flow instabilities. These two-dimensional waves are amplified and three-dimensional hair-pin vortices are formed. Finally, areas of turbulence, denoted as turbulent spots, start to develop in the streamwise direction. In bypass transition where the level of turbulence in the free-stream is high, the transition is usually seen at a significantly lower Reynolds number, and the mechanisms by which the transition occurs often involve no or little T–S waves. In these two transition mechanisms, vortical patterns within the transition region are called "coherent structures" which are responsible for skin friction drag and heat transfer increase. Another important category is the separation-induced transition, first introduced by Mayle [1]. In this mechanism, the laminar boundary layer separates under the influence of a pressure gradient and transition develops within the separated shear layer as a result of an inviscid instability mechanism. At the point that the flow reattaches, a laminar-separation/turbulent-reattachment bubble is formed on the surface.

Although there are considerable improvements in transition detection in steady flows and over the rigid structures, the effect of unsteadiness of the rotating or oscillating blades and surfaces on the boundary layer state is still ascertainable. Boundary layer transition location is a significant aerodynamic characteristic to be examined in design of modern rotorcrafts and wind turbines. The main flow features in such applications are associated with the principals of the flow over the pitching airfoils. Due to the complexity of the transition detection on oscillating airfoils and due to the lack of certain knowledge of unsteady transition, numerous designs have still relied on the steady transition characteristics. However, with the development of transition detection techniques and signal processing methods, modern designs can benefit taking the effects of unsteady transition into account. Early transition-detection methods were based on visual detection of the transition location using a variety of methods such as smoke wire technique and surface oil method [2, 3]. Currently, most pervasive measurement techniques for transition detection rely on the measurement of surface shear stress and temperature variation, which are prompted by the change in boundary layer state. For instance, measurements of shear stress fluctuations were conducted across laminar, transitional, and turbulent boundary layers on a flat plate employing hot-film probes by Owen [4]. Armistead and Keyes [5] studied local turbulence-induced fluctuations in the pipe flow of water for a Reynolds number range of 1.1×10^4 to 1.7×10^5 using flush-mounted hot-film sensors. Moen and Schneider [6] studied a shock-induced boundary layer with the aim of determination of the effect of sensor size on the performance of flush-mounted hot-film sensors. Schulte and Hodson [7] employed surface-mounted hot-film gauges for investigation in the development of the unsteady suction side boundary layer of a highly loaded low pressure turbine blade. Lee and Wu [8] presented a comparison of experimental results on transition of wall-bounded flows obtained by hot-film measurement, flow visualisations, and particle image velocimetry (PIV).

In addition, infrared thermography technique has been successfully implemented for transition detection. Horstmann et al. [9] introduced the transition location as the position where the wall shear stress is increased on a special wing glove using infrared image technique. Gartenberg et al. [10] developed an experimental method based on infrared imaging for transition detection in cryogenic wind tunnels. However, due to the presence of high frequency phenomena in transition of the pitching airfoils, the higher time resolution tools are absolutely preferred for transition detection. Hot-film anemometry is the most successful and applicable technique for capturing the unsteady transition region while other methods are applied as well. Pascazio et al. [11] employed embedded laser velocimetry measurement method for unsteady boundary layer measurements on a NACA0012 oscillating airfoil. Kim and Chang [12] studied the effect of low Reynolds number on the aerodynamic characteristics of a pitching NACA0012 airfoil. Their results indicated that an increase in Reynolds number promotes the occurrence of boundary layer events such as laminar separation and transition. Nati et al. [13] investigated the effect of a pitching motion on the characteristics of an LSB over the SD7003 airfoil using time-resolved planar and tomographic PIV where separation, transition, and vortex roll-up onset were studied. The unsteady flow on a pitching LS(1) 0417 airfoil was experimentally investigated using micro-electro-mechanical systems thermal flow sensors by Leu et al. [14] benefiting from high spatial resolutions and response times as well as minimal interference of these sensors with the flow.

Transitional boundary layer flows have been the subject of several research studies. Vlahostergios et al. [15] introduced a cubic non-linear eddy-viscosity model combined with the laminar kinetic energy to model the separation-induced transition on a flat plate with a semi-circular leading edge. Compared with the linear model, it was reported that the proposed combined model behaves better in cases where the freestream turbulence intensity is low. Suluksna et al. [16] proposed mathematical expressions for two significant parameters to control the onset location and length of transition in the $\gamma - Re_\theta$ four-equation transition model. They concluded that the correlation for the Reynolds number based on momentum thickness needs only to be expressed in terms of local turbulence intensity, so that the more complex form of the correlation that includes pressure gradient effects is unnecessary. Bernardini et al. [17] investigated the effect of compressibility on roughness induced boundary layer transition up to Mach number 4 by considering variations in the roughness height using direct numerical simulations. They found an identical vortex organization for all flow cases that experience transition, regardless of the Mach number. It was the generation of streamwise and wall-normal vorticity with the formation of an unstable detached shear-layer on the top of the element. Serna and Lázaro [18] experimentally investigated the laminar separation bubble (LSB) using laser based flow diagnostics. Proper understanding of the boundary layer state and transition point location is required in the aerodynamic design of air vehicles, and it has been the main incentive for many researchers ([19–21]). Kubacki and

Dick [22] presented a simple algebraic model for laminar to turbulent transition in boundary layers subjected to elevated free-stream turbulence. The model was combined with the k-ω RANS turbulence model by Wilcox. The transition model included the effects of both filtering of high-frequency free-stream disturbances by shear and breakdown of near-wall disturbances into fine-scale turbulence. Qingqing Ye et al. [23] studied the boundary layer transition over isolated roughness elements in the incompressible flow regime using tomographic PIV. To compare the different flow topologies and study the effect of the element shape on accelerating boundary layer transition, four different geometries (cylinder, square, hemisphere and micro-ramp) were considered maintaining constant height. Medina et al. [24] conducted a new model for predicting pretransitional boundary layer fluctuations using the laminar kinetic energy concept for representing them into the OpenFOAM solver.

Unsteady boundary layer transition on oscillating airfoils has been characterised for a range of pitch rates and Reynolds numbers using hot-film anemometry. Surface shear-stress measurements were conducted by Kiedaisch and Acharya [25] on pitching NACA0012 airfoil at a constant rate form 0 to 45° using array of hot-film sensors. Unsteady boundary layer reversal and transition on a NACA0015 airfoil were studied by Schreck et al. [26] for a range of pitch rates and Reynolds numbers whit the aim of determination of the unsteady flow physics crucial for control of the dynamically separated flows. Lee and Basu [27] measured the unsteady boundary layer features over a pitching NACA0012 airfoil within and beyond the static-stall angle. They indicated that the pitch up motion assists to keep the boundary layer laminar at a higher angle of attack in comparison to that could be attained in static condition. Transition processes in the boundary layer of a high-pressure turbine rotor blade were investigated by Tiedemann and Kost [28]. The results were based on time-resolved, qualitative wall shear stress data, which was derived from surface hot-film measurements. Lee and Gerontakos [29] investigated the characteristics of the unsteady boundary layer and stall features on an oscillating NACA0012 airfoil using closely spaced multiple hot-film sensor arrays at $\mathrm{Re} = 1.35 \times 10^5$ with particular attention to the spatial-temporal progression of the location of the transition and separation. Yarusevych et al. [30] conducted a series of experiment on transition of NACA 0025 airfoil. They observed that laminarly separated shear layer fails to attach to the surface in lower Reynolds number, but it leads to reattachement in higher one. Since the experimental results and the linear stability theory were in a good agreement, they figured out that the formation of the roll-up vortices can be essentially considered inviscid in nature. Masdari et al. [31] carried out an experimental investigation on a supercritical airfoil, calculating the boundary layer velocity profile and its dominant frequencies. They found that there is a frequency mode at which the oscillation frequency of the airfoil is the dominant frequency and functions as a factor causing turbulence in relation with the amplitude of oscillation of the airfoil. Also, Tabrizian et al. [32] performed a discrete wavelet transform on collected data from a boundary layer velocity profile of a supercritical airfoil in a pitch-hold-return motion. They resolved a vortex formation frequency inside boundary layer during upstroke motion. Rudmin et al. [33] presented a method for laminar separation and transition detection over a slowly pitching airfoil, with a frequency of 0.025 Hz, based on hot-film sensors responses. The proposed method was based on the windowed correlation between adjacent hot-film signals and the observation of the signal spectra but only applied on the static and the quasi-static cases. The same detection method was applied on a pitching airfoil to study the boundary layer behavior, and results were compared against the results obtained from Large Eddy Simulation (LES) [34]. Tatar et al. [35] investigated the effects of reduced frequency on the transitional boundary layer over a NACA0012 pitching airfoil using intermittency-based $k - \omega$ shear stress transport model. They reported a delay in the chordwise boundary layer transition point by increasing the reduced frequency and a vortex shedding within the LSB. Gardner and Richter [36] presented a method based on the analysis of the standard deviation of the surface pressure distribution for unsteady transition detection. The peak in the standard deviation of the pressure distribution is used as a measure of the transition position. The method was further developed to an analysis algorithm utilizing the skewness for the detection of the transition on the pitching airfoil DSA-9A from the hot-film data [37].

As noted above, extensive studies have been conducted on detecting boundary layer transition over the moving airfoils. However, most of the studies focused on the "common" geometries such as NACA series airfoils. In the present work, efforts were made to study boundary layer transition onset over a pitching supercritical airfoil at off-design flow condition. Supercritical airfoils were designed to reduce drag at high transonic regime by means of a mostly-flat upper surface and a big curvature is also considered at the lower surface near the trailing edge to compensate the lift loss caused by flat upper surface. This causes an unknown behavior of this type of airfoils at incompressible flow regime and Reynolds number lower than that of the design point. Hot-film measurements over the upper surface of a supercritical airfoil which undergoes sinusoidal pitching motions at $\mathrm{Re} = 8.11 \times 10^5$, are presented and the effects of reduced frequency and mean angle of attack are studied. More interestingly, versatile methods for transition detection are examined along with an automatic algorithm for peak capturing in order to prevent bias on transition detection. Moreover, time–frequency analysis is performed to find out the frequency content and evolution of the transition mechanism. A proper wavelet method is employed to investigate the emerged frequencies during the transition in spatial-temporal domain. The analysis enables one to achieve a range of existing and emerging frequencies in transition process over a cycle of oscillation. Using wavelet method to capture dominant frequencies in shear layer and during the transition is a novel method that will be discussed further in this study.

2. Experimental apparatus

The tests were conducted in an open test section Gottingen-type wind tunnel with the maximum turbulence intensity of 0.4% at 35 m/s and at where the model was located. To reduce the open test section jet effects and to assure that the flow uniformity is within an acceptable range, a temporary wooden test section (2.5 m $\times$ 1 m) is placed just after the contraction outlet. A stainless steel straight section of a supercritical airfoil (RAE5215) with the chord of 40 cm was selected to investigate the transition behavior over its upper surface. The model had the maximum thickness of 9.8% and was installed vertically in the test section along with two 1m-diameter end plates in order to guarantee the two-dimensional flow condition, occupying about 2.5% of temporary test section frontal area while stayed at 8° AOA. Also, to ensure the 2D flow over the airfoil, the mean flow uniformity has been examined over 30% of airfoil's span from mid section containing the region where the hot-film arrays were installed. For the test condition, the Reynolds number was obtained about 8.11×10^5 based on the free stream velocity and the airfoil chord. Figure 1 shows the airfoil section.

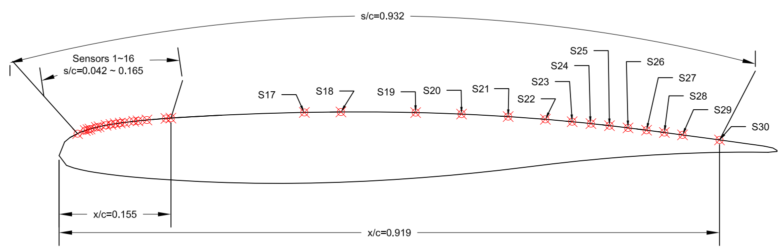

Figure 1: The airfoil section and the hot-film sensors location.

The upper surface was covered with two sheets of Senflex™ hot-film arrays having 64 and 100 sensor elements with the normal elements spacing of 0.1 inches. However, the 64-element sheet had half sensor spacing at the middle and was attached to the forward section of upper surface where the transition region was expected to be emerged. Also, the 100-element sheet was adhered just behind the first sheet in a manner that ensured all the sensors were in the same direction over the upper surface (Fig. 2). Moreover, there were restrictions on the quantity of hot-film sensors and more spacing was considered between the sensors on the upper surface at some points. Nevertheless, it is worth nothing that the sensors' arrangement has provided the ability of transition detection and more future investigations.

A 30-channel constant temperature anemometer complete with a 16-bit em-

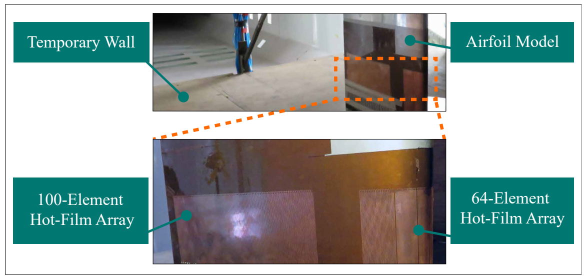

Figure 2: Airfoil model with hot-film sensors in the open test section.

bedded data acquisition system was employed to commission the hot-film sensors and the output voltages were collected at the rate of 2.4 kHz. Also, the set-up was equipped with an output trigger of 3.3 V, transmitted immediately after the start of data acquisition. This trigger signal was important to synchronize the hot-film outputs with the instantaneous angle of attack. The connection diagram and the sequence of the events are shown in Fig. 3.

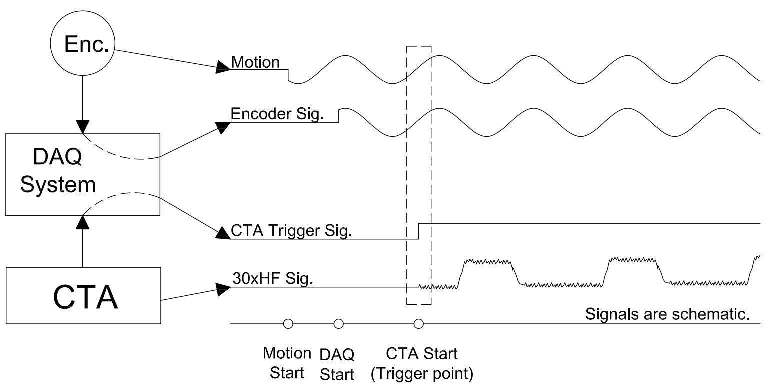

Figure 3: Data acquisition configuration and timeline.

A 750 W servo motor along with a proper drive were used to generate the pure pitching motion via a four-bar linkage mechanism, capable of producing pitching oscillation with the maximum frequency of 5 Hz. Figure 4 depicts a schematic of the pitching oscillation mechanism and the equation of motion is as Eq. (1). The value of instantaneous angle of attack was measured by a 12-bit differential rotary shaft encoder, directly connected to the airfoil shaft at quarter chord. Utilizing the CTA output trigger, the encoder output was acquired concurrently with those of hot-films.

$$\alpha = \alpha_0 + \alpha_{\mathrm{amp}}\ sin(\omega\ t) \tag{1}$$

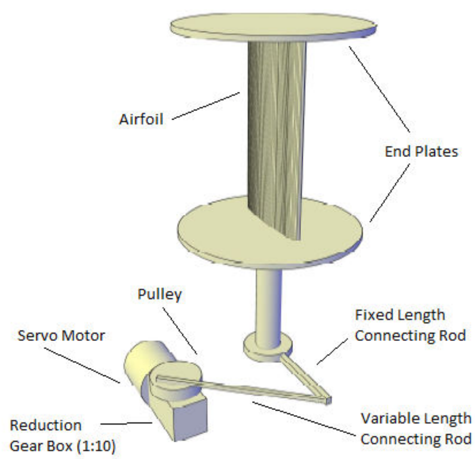

Figure 4: The pitching oscillation mechanism.

A process of uncertainty analysis was performed at the confidence level of 95% and the maximum uncertainty of output voltages was obtained 2.5%, comprising both bias and precision errors.

3. Results and discussion

Development of boundary layer is investigated on the upper surface of the supercritical airfoil using hot-film sensors. The airfoil is oscillated sinusoidally around its quarter-chord. Results are presented for three reduced frequencies of 0.017, 0.035, and 0.053 and two mean angles of attack of 0° and 4°. For all cases, the amplitude of pitching oscillation is selected equal to 4° at which the transition was expected. Table 1 presents the test plan. Hereafter, the cases with α_0=0 and α_0=4° may denote as case 1 and case 2, respectively. At the beginning of this section, several transition and relaminarization detection methods are verified. Also, the behaviour of the flow and corresponding events are described. Then, the influence of reduced frequency and mean angle of attack on the transition and relaminarization locations are studied. Eventually, a temporal-spatial frequency analysis is employed, utilizing continuous wavelet transform in order to provide a valuable insight to the existing phenomena over the pitching airfoil.

Table 1: Test plan

Test case	α_0 (°)	α_{amp} (°)	k
1	0	4	0.017, 0.035, 0.053
2	4	4	0.017, 0.035, 0.053

3.1. Transition point detection algorithms

Hot-film anemometry is one of the well-known techniques for unsteady boundary layer transition detection. A traditional way of transition detection using hot-film is to manually extract the detail of the transition from laminar to turbulent flow from phase-averaged voltage signal of individual sensors and through the visual interpretation of the changes in voltage levels. However, this manual procedure demands both time and skill. Alternatively, a detection method was developed allowing a computer-aided automated transition detection based on the skewness of data. Skewness is a statistical characteristic and indicates the level of asymmetry of the signal around its mean. The approach was earlier implemented for determining the boundary layer state by Tiedemann [28]. In addition to the skewness, other detection methods such as standard deviation of the phase-averaged signal and the signal derivative have also been verified here to assess the functionality of these methods in detection of the unsteady boundary layer transition. The skewness, standard deviation, and derivative of a hot-film signal at $s/c = 0.165$ are shown in Fig. 5, respectively below the main hot-film signal where the airfoil oscillates with the reduced frequency of 0.017, and around the mean AOA of 4°. The time is normalized with the period of oscillations (T) to show the time of occurrence of boundary layer phenomena, e.g., transition and relaminarization, in a cycle of airfoil oscillations. The skewness and standard deviation are evaluated utilizing a sliding window with the width of 5% of the period. It is worth noting that in Fig. 5 the results are presented in such a way that the minimum AOA occurs at $t/T = 0$ and $t/T = 1$, and the maximum AOA is at $t/T = 0.5$. As depicted in Fig. 5, the flow is purely laminar at $t/T \leq 0.21$ and $t/T \geq 0.81$ and purely turbulent at $0.31 \leq t/T \leq 0.72$. Distribution of data in a single window is nearly normal, while at the start of transition, a sudden increase in the voltage signal leads to a deviation of the skewness from zero towards the positive values and a sudden rise in the standard deviation. A positive skewness in transition and near the laminar regions is due to the presence of a few number of disturbances with the high voltage values that cause the right tail of normal distribution to be longer. Near the turbulent region, however, the number of turbulent spots increases and the mode of data becomes greater than its mean, therefore the left tail is longer this time and the skewness returns negative values. At 50% intermittency, where the flow is literally in a balance between laminar and turbulent, the voltage distribution in a single window is almost symmetric. Hence, the skewness approaches zero again. Standard deviation, however, is rocketing. With the start of turbulent flow and fluctuation of the data in a window around its mean, the standard deviation decreases, and the skewness goes back to zero from negative values. It can be seen in Fig. 5 that the start and the end of laminar and turbulent flows are not accurately predicted from the skewness of the voltage signal where the standard deviation comparatively results in more reliable outcomes. The derivative of the signal using a central differencing approach obtains the most accurate points for the start and end of the fully laminar and turbulent flows. It should be noted that the selection of the window width is significant. With a low-width window, the skewness and standard deviation may manifest huge fluctuations, making it very difficult to extract desired (start and end) points from the obtained signals. Also, as it is seen in Fig. 5, the implementation of a moderate width is more plausible for indicating the 50% intermittency point, since it better represents the existence of both laminar and turbulent flows at a specific period of time. Moreover, the peak of derivative does not make any physical sense to be a good criterion for 50% intermittency. Accordingly, in this study, the derivative of the voltage signal is used for extracting the start and the end of the laminar and turbulent flows, while the standard deviation is implemented for indicating the 50% intermittency.

3.2. Transition and relaminarization phenomena over the upper surface

The voltage signals of the sensors on the upper surface of the airfoil are demonstrated in Fig. 6 for the case 2 with the reduced frequency of 0.017. Also, the 50% intermittency locations during the transition and the relaminarization are marked on the figure. Near the leading edge, the presence of an LSB is notable at about $0.31 < t/T < 0.68$. A gradual increment of AOA causes an improvement of an adverse pressure gradient near the leading edge and the formation of the LSB. As a consequence of the laminar flow separation, the skin friction and hot-film heat transfer levels are reduced, and so, the level of voltage is declined. This region over the upper surface, marked as region 1 in the figure, experiences neither transition nor turbulent flow during the whole pitching cycle. However, with decrement of the AOA, the LSB vanishes and the the flow reattaches to the surface in a laminar state. Also, a little farther from the leading edge, at $s/c = 0.087 \sim 0.165$ another voltage decay is detected which again represents formation of a separation bubble (at region 2) that usually emerges at the suction side of the airfoil caused by the same mechanism. In this case, the LSB lasts for a shorter time and is pursued by the transitional and turbulent regions evinced by a jump (region 3) to a higher levels of voltages with more fluctuations (region 4), respectively. The transition process starts with a sudden change in voltage right after the laminar state (region 7), but ends to turbulence with a slight voltage change. It is obvious that the LSB moves forward and stays more time on the airfoil surface as the AOA rises. It seems that its length is greater at higher angles, as well. After a period of

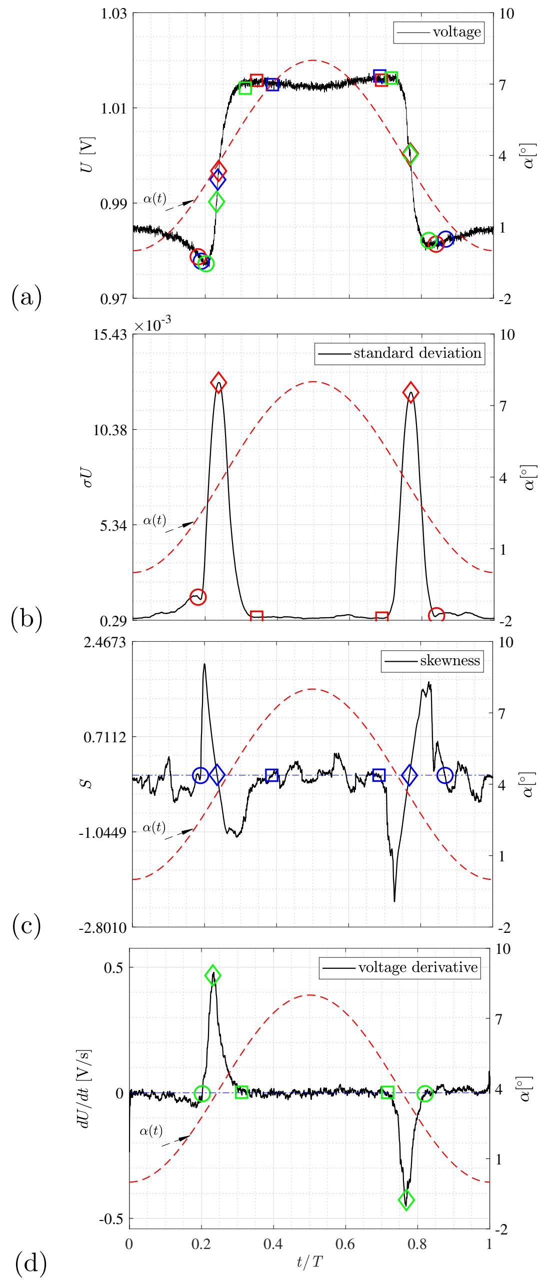

Figure 5: (a) Voltage signal, (b) skewness, (c) standard deviation, and (d) voltage derivative for the sensor at $s/c = 0.165$ on the upper side; Case 2, $k = 0.017$. Start/end laminar flow: circle, 50% intermittency: diamond, start/end turbulent flow: square. Blue, red, and green markers indicate the points extracted from skewness, standard deviation, and voltage derivative, respectively.

turbulence on the surface, the relaminarization takes place in a reverse process of the transition. As the AOA decreases, the relaminarization (region 5) followed by a small separation region (region 6) and eventually laminar flow appears on the airfoil surface. The relaminarization process actually happens because of the presence of a favorable pressure gradient which completely collapses the turbulence. Moreover, a region of turbulent separation can also be observed on the sensor located at $s/c = 0.932$ (region 9). As depicted in the figure, by increasing the AOA, the turbulent flow separates from the upper surface which is evinced by a slight reduction in the voltage of the signal.

Looking more accurate through the signal, for instance at $t/T < 0.2$, indicated by line (a), the flow is laminar on the upper surface for approximately 35% of the chord. However, some spikes are emerged in the signal which are amplified with getting closer to the trailing edge. This process ends up in a turbulent region at $s/c = 0.854$. The gradual amplification of the perturbations may initially be attributed to the amplification of the T-S waves as the mechanism for the natural transition to turbulent flow. At $t/T < 0.3$, designated by line (b), it is observed that the laminar flow passes over the upper surface and near the leading edge. At $s/c = 0.081 \sim 0.132$, the LSB is formed, and followed by a wide turbulent region up to $s/c = 0.88$. Then, a small separation of the turbulent boundary layer is perceived. At $t/T = 0.5$, traced by line (c), a separation bubble at the near-leading edge region is pursued by a turbulent flow at $s/c = 0.081$ and further.

Also, near the trailing edge, at $s/c = 0.777 \sim 0.88$, a number of turbulent bursts is noticeable at low AOA below $t/T = 0.11$ accompanying with a large portion of the fully turbulent flow in a period (region 8).

Apparently, two possible mechanisms of the boundary layer transition can be inferred from the behaviour of hot-film signals. Near the leading edge (lower s/c), a drop in the signal level flaunted just before its rise, introducing the occurrence of the LSB. However, moving towards the trailing edge at low t/T where no LSB exists, a gradual amplification is observed for the signal level of the laminar to that of the turbulent regime. This reflects a transition mechanisms,

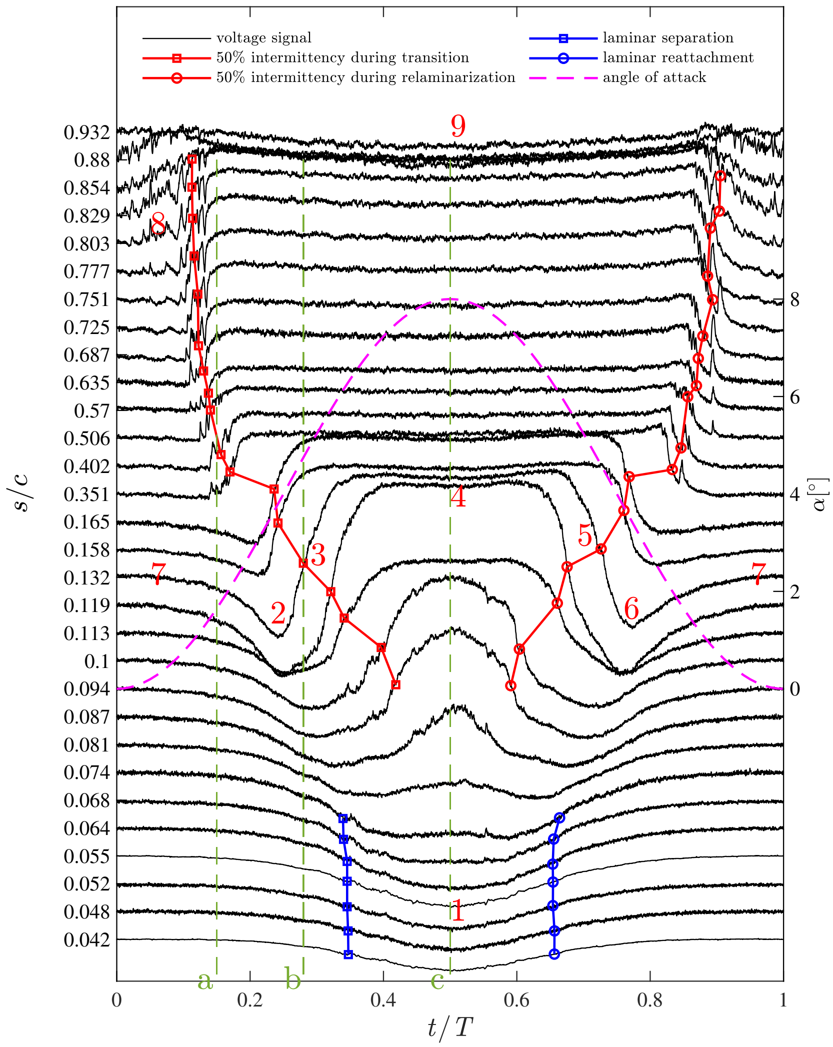

Figure 6: Voltage signal for all sensors on the upper surface of the airfoil; Case 2, $k = 0.017$. The vertical green dashed lines of a, b, and c represent t/T equal to 0.15, 0.28, and 0.5, respectively.

perhaps the natural one, which is completely different from the separation-induced transition process.

In Fig. 7, the movement of transition and relaminarization points on the upper surface is shown for the same previous case. As it was mentioned earlier, the start and the end of the transition region are identified using the derivative of the signal, and the 50% intermittency is marked as the peaks in the standard deviation of the signal. Whereas, by increasing the AOA the transition location is moved towards the leading edge, it is moved backward to the trailing edge while the AOA decreases. This generates a hysteresis between the upstroke and downstroke motions. In this case, the transition region moves on the upper surface between $s/c = 0.087$ and $s/c = 0.88$; however, at $s/c = 0.88$, the flow is uncertain between laminar and turbulent states at minimum AOA. Approaching to the trailing edge, no laminar flow is seen at $s/c = 0.932$ and the boundary layer becomes fully turbulent. The rate of the transition region movement is fast during the first quarter of the oscillation cycle as the 50% intermittency point moves from $s/c = 0.88$ at $t/T = 0.043$ to $s/c = 0.165$ at $t/T = 0.235$. Thereafter, it reduces during the second quarter of the cycle. In other words, there is a sudden change in the transition location before the 2° AOA which can be ensued from the flatness of the upper surface. Furthermore, the fraction of time of motion in which the boundary layer is fully turbulent is larger near the trailing edge positions compared to the ones at the leading edge.

3.3. Influence of the reduced frequency

The influence of the reduced frequency on the unsteady transition region is described in this section. First of all, as the airfoil chord and the freestream velocity were constant during the tests, the only effective parameter on reduced frequency is the pitching motion frequency. The airfoil oscillates with three reduced frequencies of 0.017, 0.035, and 0.053 and the results are presented for different oscillations. Locations of the 50% intermittency are shown over the upper surface of the airfoil and the extent of the turbulent region and the time delay between the transition movement and the airfoil motion are exhibited.

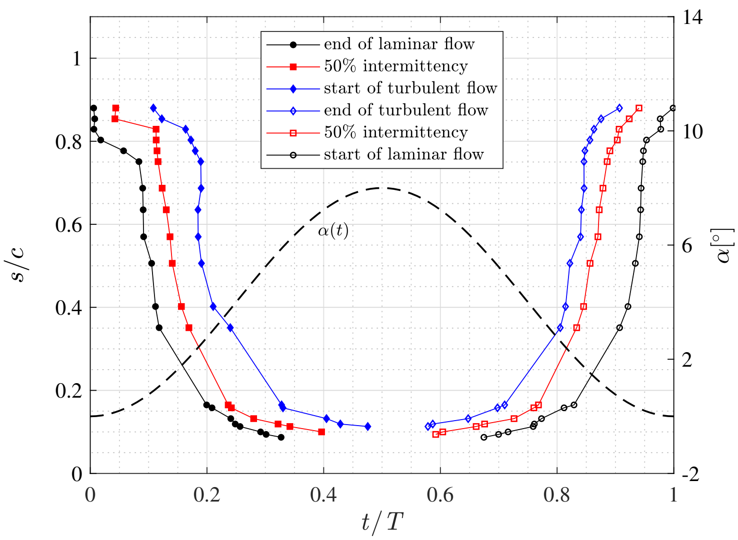

Figure 7: Variation of transition locations vs. the time; Case 2 for $k = 0.017$.

The transition locations against the non-dimensional time and the AOA, are depicted in Fig. 8 $\sim$ Fig. 9 for oscillations of the case 1 and 2, respectively. As figures reveal, variation of the reduced frequency strongly affects the transition characteristics. An increase in k leads to a delay in the transition onset, postponing it to a higher AOA; this results in a wider hysteresis between the upstroke and downstroke motions. The delay can be related to the apparent mass and unsteady features in the boundary layer which is more tangible as the k rises. For the sensor located at $s/c = 0.635$ in case 2, this time lag is about 0.07 t/T between the oscillations with reduced frequencies of 0.017 and 0.035. For the oscillation with $k = 0.017$, transition and relaminarization happen nearly at the same angle of attack. Also, the pattern of the transition and relaminarization are almost symmetric with respect to the AOA. The more the k increases, the more the asymmetry appears in the pattern. As the lowest k is presumed to be in quasi-steady regime, the up/down strokes are roughly identical and are in a good agreement with the static result. However, as the reduced frequency rises, the corresponding apparent mass causes a wider hysteresis loop. Moreover, the trend of the transition movements are very similar for all frequencies in spite of the range of reduced frequencies. Additionally, for the negative angles of attack the transition region is placed near the trailing edge and mild variation in its location is observed.

Case 2 has less agreement with the static condition in comparison to first case. This might be as a result of the fact that at higher AOA (greater than 2 degrees) the location of 50% intermittency points are so close together and to the leading edge. Meanwhile, the airfoil motion makes a noticeable change in transition location as well. In addition, at higher reduced frequencies, a very rapid change in the location of the transition and relaminarization points is detected which can be called a rapid transition/relaminarization jump.

Figure 10 demonstrates time history of the hot-film signals for the oscillation case 2 and three reduced frequencies at $s/c = 0.75$. Some spikes are revealed by the signals which reflect formation of a vortex-like disturbance or a circulation region. As a result, a surge in the level of heat transfer is expected. They emerge at a moment and vanish a moment later, therefore they appear as spikes. However, by increasing the reduced frequency, the signal's spikes diminish. Alternatively stated, a rise in the frequency of the pitching motion yields weakening or omission of such disturbances. As k increases, the existence of time lag which is an important inherent subject in unsteady flows is revealed. The trend of hot-film signal is slightly shifted to the right (higher instants), compared to variation of the angle of attack, reflecting a lag in hot-film response as to the motion. Hence, the flow faces to an angle of attack smaller than the actual one. Despite the lower k that the level of hot-film output declines at higher AOAs, implying the turbulent separation, no decrease is seen for the higher k. It is worth nothing that the same observations are found for the relaminarization process.

3.4. Influence of mean angle of attack

Figure 11 demonstrates the transition and relaminarization points against the AOA for the oscillating airfoil with mean AOAs of zero and 4 degrees, at three reduced frequencies. For the higher mean AOA, the flow experiences

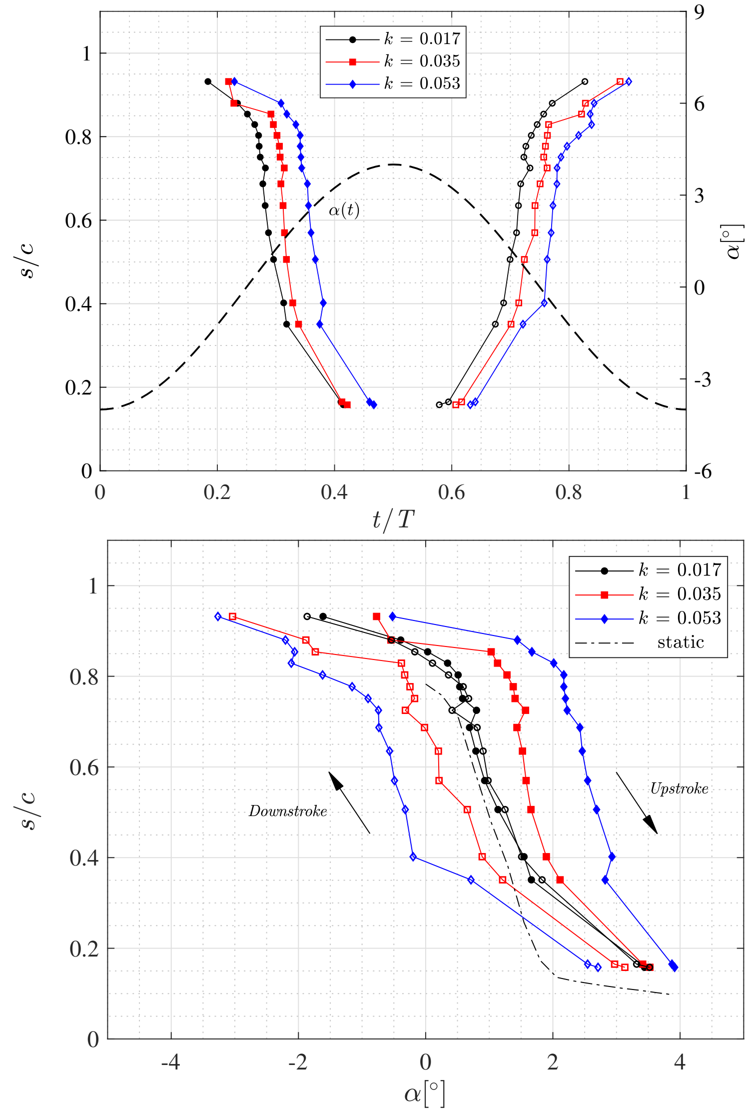

Figure 8: Variation of transition locations versus time (top) and angle of attack (bottom) for oscillation with various frequencies; Case 1.

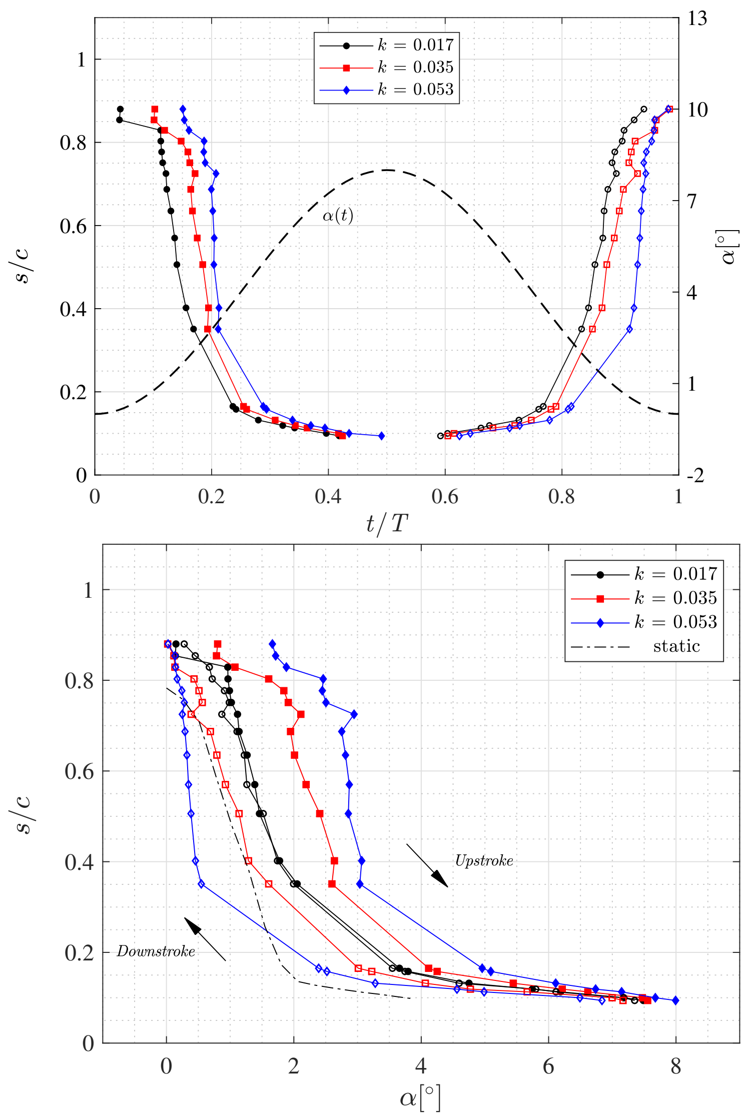

Figure 9: Variation of transition locations versus time (top) and angle of attack (bottom) for oscillation with various frequencies; Case 2.

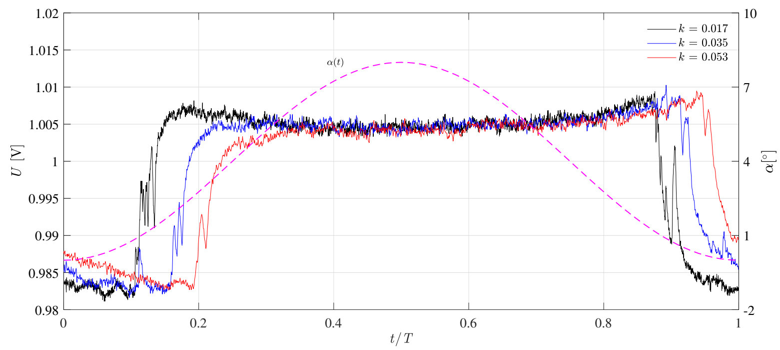

Figure 10: Hot-film signals at three reduced frequencies at $s/c = 0.75$, Case 2

turbulence over a more portion of a cycle which was expected due to higher AOAs through which it passes. Moreover, at the k=0.017, variation of the transition onset is broadly similar for both cases. Nevertheless, transition occurs slightly in higher AOAs for $a_0 = 4°$. Although for the lower k which is quasi-steady, no significant change in pattern of the transition and relaminarization is detected, for the higher reduced frequencies transition and relaminarization points move slightly faster in the case 2. On the other hand, for the higher k, the transition process is almost similar for both mean angles of attack, while the relaminarization begins faster for case 2. Indeed, the relaminarization point for AOAs less than 1°, dramatically moves towards the trailing edge in case 2, for instance, at zero AOA, the relaminarization point for case 1 is about $s/c = 0.4$, while for case 2, it is close to the trailing edge. Conversely, as depicted in Fig. 11, the location of relaminarization for negative AOAs gradually moves towards the trailing edge. The location of this slope-change appears with a lag for higher frequencies, though.

3.5. Time-Frequency Analysis

Wavelets, introduced by Grossmann and Morlet [38], have been extensively adopted in many areas of science and engineering. In fluid mechanics, wavelets were first used in the early 1990s to analyze turbulent flows ([39] and [40]). Continuous wavelet analysis can be used to study how spectral features evolve over time, identify common time-varying patterns in signals, and perform time-

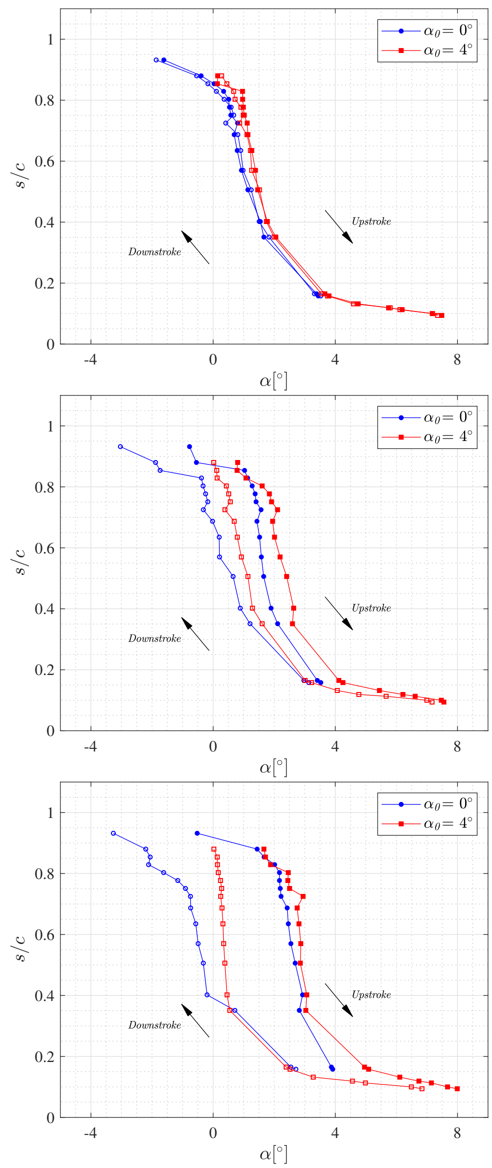

Figure 11: Variation of transition locations versus α for oscillations with two mean angles of attack and three reduced frequencies; k = 0.017 (top), k = 0.035 (middle), k = 0.053 (bottom).

localized filtering. In the present study, the complex Morlet wavelet ([38]) is used to analyze hot-film signal at each sensor position. The wavelet transform is given as:

$$\varphi\left(t\right)=\frac{1}{\sqrt{4\pi}}e^{2i\pi f_0 t}e^{-t^2/2} \tag{2}$$

and the wavelet transform coefficients are defined as:

$$C\left(a,b\right)=\frac{1}{\sqrt{a}}\int_{-\infty}^{+\infty}U\left(t\right)\varphi^{*}\left(\frac{t-b}{a}\right)dt \tag{3}$$

Figure 12 shows the absolute value of the wavelet transform coefficients for 8 locations over the upper surface during a period of motion for case 2 at $k=0.017$. Also included in the plots, are the hot-film sensors output.

Regarding Fig. 12, at $s/c=0.048$, the level of signal first decreases due to the presence of the leading edge laminar separation bubble where the local velocity of the flow and hence the wall shear stress lessen. The corresponding wavelet content shows a very low frequency, almost steady, low intensity spots representing the bubble region. At $s/c=0.068$, the same events are exhibited. Compared with the previous position, the level of signal as well as frequency components are grown. This phenomenon can denote the initiation of the flow fluctuations within the concept of "laminar-kinetic-energy" which was proposed by Mayle and Schulz [41]. A clear strengthen of low frequencies, within the range of 10-15 Hz., is seen for this location. Moving toward the trailing edge on the upper surface, it appears that the boundary layer transition first occurs at $s/c=0.094$. The separated flow is reattached in the turbulent state for a short period after which a relaminarization process has occurred during the down-stroke motion (in which the level of hot-film signal is changed to its laminar value). A region with considerable wavelet magnitude at about the frequency range of 10-70 Hz. implies such a sharp variation with wide frequency content at around $t/T=0.5$. More accurate, the higher portion of this range belongs to the transition events while the lower ones are concurrent with the LSB. It seems that very short region of turbulence causes the transition and relaminarization frequencies to be merged and appear as a peak region at this point.

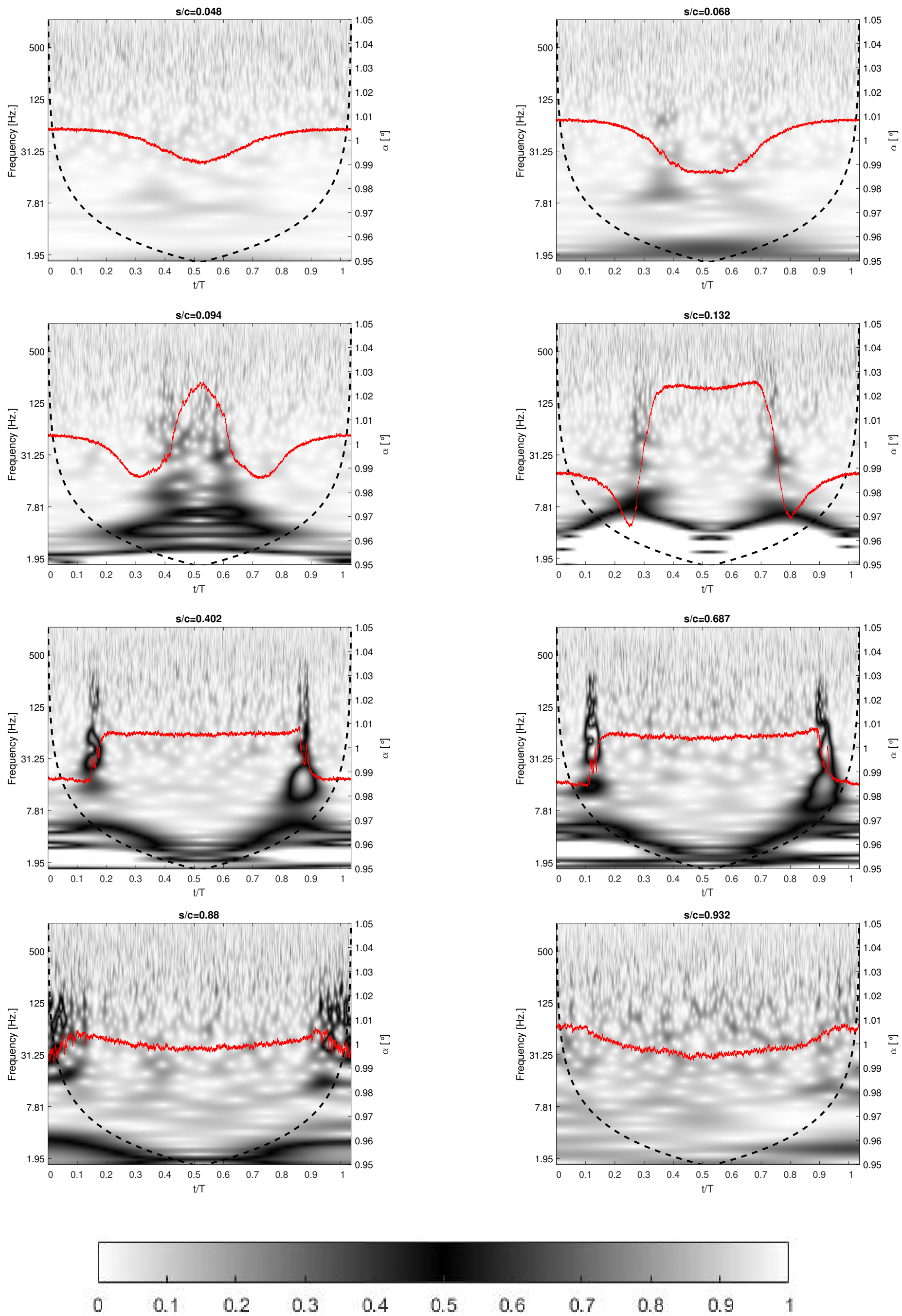

Figure 12: Contours of wavelet transform coefficients magnitudes along with hot-film signals at different positions over the upper surface

Farther down from the leading edge at $s/c = 0.132$, transition is captured with more turbulent state of the boundary layer during the motion in Fig. 12. It is worth nothing, compared with other cases that the amount of hot-film signal variations is the most significant, in both separation and reattachment states at this location. This implies existence of the LSB core which is pursued by the highest magnitude of shear stress. The development of the wavelet transform coefficient at this point shows a high frequency content within the laminar separation bubble with diverse amplitudes. This behaviour is in agreement with the experimental [42] and DNS [43] visualisation results, and is due to vortex shedding within the laminar separation bubble zone. Jumping into $s/c = 0.402$, one may perceive a more turbulent portion of the boundary layer state which has been expected due to being farther from the leading edge of the airfoil. The level of changes in hot-film signal in both laminar separation and reattachment moments are not as much as the previous point, which resembles this point to be far from the laminar separation bubble core. Rapid change of signal is also another important feature at this point exciting a great frequency interval of 25-210 Hz. Focusing on the raise part of the signal, it can be found that there is no separation zone after the laminar boundary layer since no signal decline can be observed when transitioning from the laminar to the turbulent state. As stated before, this indicates another transition mechanism which is different from the LSB. Here, the variety of dominant frequencies during different transition mechanisms is revealed. As demonstrated, the phenomena at LSB transition mechanism are relatively in lower range than those of the other mechanism. The same features are observed at $s/c = 0.687$. However, the interval of fluctuation frequencies in the signal is increased to 12-280 Hz. representing the amplification of coherent structures such as the turbulent spots or flow streaks. For instance, a high amplitude fluctuation is observed at about $t/T = 0.12$ and around the 50% intermittency point in the transition process which may contain dominant frequencies of approximately 37 and 61 Hz. More interestingly, the same phenomenon recurs with an identical frequency in the relaminarization process. However, generally having focused on the two latter locations, an asymmetry is clearly observed in frequency content of these locations expressing the difference between the transition and relaminarization processes.

Moving more towards the trailing edge, the characteristics of the hot-film signal at $s/c = 0.88$, it seems that regions with greater intensity of the wavelet transform belong to the small laminar zones of the signal at the initial and final instances of the motion. The flow is separated in the turbulent state at this point yielding in lower skin friction and signal level. Also at $s/c = 0.932$ the flow seems to be fully separated roughly over the whole cycle and accordingly no particular phenomenon is felt on the surface.

At last, it should be noticed that below the dashed-line of Fig. 12, information in the scalogram should be treated as suspect due to the potential for edge effects. Above the dashed-line, the information provided by the scalogram is an accurate time-frequency representation of the data. This arises from non-existence of mathematically precise rule to determine the extent of the unreliability at each scale [44, 45].

4. Conclusion

A series of experimental tests were performed to figure out the behaviour of boundary layer transition over a pitching supercritical airfoil using hot-film sensors. The influences of reduced frequency and mean angle of attack were studied where, the start and the end of the transition and relaminarization were captured by the peak point in signal derivative and the 50% intermittency was obtained from the peak in standard deviation.

Two different transition mechanisms were recognized from the measurements. Laminar separation bubble was identified as the transition mechanism near the leading edge of the airfoil ($s/c < 0.156$) and at higher AOAs ($\alpha > 1°$). Moving toward the trailing edge, the size and strength of the bubble were deemed to become shorter and weaker, so that at $0.351c$ downstream of the leading edge, no bubble was found on the surface. At low AOAs, mostly less than $1°$, however, the cause of boundary layer transition was differed from the bubble. In essence, decrement of AOA is accompanying with the relaminarization process generated by presence of favorable pressure gradient. Also, on the last sensor near the trailing edge and at $s/c = 0.932$, signals of turbulent separation were seen at high AOAs. Increasing the reduced frequency eventuated in few results out of which are a delay in transition onset up to $0.07t/T$ at $s/c = 0.932$ in case 2 and postponing it to a higher angle of attack, widening the hysteresis between the upstroke and downstroke motions and weakening or omission of vortical disturbances ensuing the removal of spikes in the signals.

The effects of mean AOA on movement of transition and relaminarization points were studied, indeed. For higher k the relaminarization point moves faster in higher mean AOA, while this process slowed down at negative AOAs. As expected, no important change was detected at lower k where the flow presumed to be quasi-steady.

An increase in the level of signal along with formation of higher frequency components (10 to 15 Hz.) while the state of flow is still laminar, implied development of the streamwise fluctuations and the concept of "laminar-kinetic-energy". The frequency content within the laminar separation bubble confirmed the presence of vortex shedding and nonlinear modes interaction within the transition region. The existence of another mechanism is also implied by the higher frequencies (up to 210 Hz.) emerge at the points farther from the leading edge. Furthermore, the wide range of frequencies in the transition and relaminarization processes introduced the fact that multiple different coherent structures are produced in boundary layer. Finally, a time-frequency analysis showed that an asymmetry existed between the frequency content of the upstroke and downstroke motions, implying the difference between the transition and relaminarization processes especially at locations farther down from the bubble zone toward the trailing edge.

References

[1] R. Mayle, The role of laminar-turbulent transition in gas turbine engines, International Gas Turbine and Aeroengine Congress and Exposition 77 (1991) 500–520. doi:10.1017/S0022112004009851.

[2] J. Cornish, A Device for the Direct Measurements of Unsteady Air Flows and Some Character istics of Boundary Layer Transition, Mississippi State University, Aerophysics Research Note 24 (1964).

[3] W. A. Cassels, J. F. Campbell, Boundary-layer transition study of several pointed bodies of revolution at supersonic speeds, Vol. 6063, National Aeronautics and Space Administration, 1970.

[4] F. Owen, Fluctuation and transition measurements in compressible boundary layers, in: 26th American Helicopter Society, Annual National Forum, American Institute of Aeronautics and Astronautics, Reston, Virigina, 1970. doi:10.2514/6.1970-745.

[5] R. A. Armistead, J. J. Keyes, A Study of Wall-Turbulence Phenomena Using Hot-Film Sensors, Journal of Heat Transfer 90 (1) (1968) 13. doi:10.1115/1.3597444.

[6] M. J. Moen, S. P. Schneider, The Effect of Sensor Size on the Performance of Flush-Mounted Hot-Film Sensors, Journal of Fluids Engineering 116 (2) (1994) 273. doi:10.1115/1.2910266.

[7] V. Schulte, H. P. Hodson, Unsteady Wake-Induced Boundary Layer Transition in High Lift LP Turbines, Journal of Turbomachinery 120 (1) (1998) 28. doi:10.1115/1.2841384.

[8] C. B. Lee, J. Z. Wu, Transition in Wall-Bounded Flows, Applied Mechanics Reviews 61 (3) (2008) 030802. doi:10.1115/1.2909605.

[9] K. H. HORSTMANN, A. QUAST, G. REDEKER, Flight and wind-tunnel investigations on boundary-layer transition, Journal of Aircraft 27 (2) (1990) 146–150. doi:10.2514/3.45910.

[10] E. GARTENBERG, W. G. JOHNSON, R. E. WRIGHT, D. L. CARRAWAY, C. B. JOHNSON, Boundary-layer transition-detection in a cryogenic wind tunnel usinginfrared imaging, AIAA Journal 30 (2) (1992) 444–446. doi:10.2514/3.10936.

[11] M. Pascazio, J. Autric, D. Favier, C. Maresca, Unsteady boundary-layer measurement on oscillating airfoils - Transition and separation phenomena in pitching motion, in: 34th Aerospace Sciences Meeting and Exhibit, American Institute of Aeronautics and Astronautics, Reston, Virigina, 1996. doi:10.2514/6.1996-35.

[12] D.-H. Kim, J.-W. Chang, Low-reynolds-number effect on the aerodynamic characteristics of a pitching naca0012 airfoil, Aerospace Science and Technology 32 (1) (2014) 162 – 168. doi:https://doi.org/10.1016/j.ast.2013.08.018.

[13] A. Nati, R. de Kat, F. Scarano, B. W. van Oudheusden, Dynamic pitching effect on a laminar separation bubble, Experiments in Fluids 56 (9) (2015) 172. doi:10.1007/s00348-015-2031-6.

[14] T. Leu, J. Yu, J. Miau, S. Chen, MEMS flexible thermal flow sensors for measurement of unsteady flow above a pitching wind turbine blade, Experimental Thermal and Fluid Science 77 (2016) 167–178. doi:10.1016/J.EXPTHERMFLUSCI.2016.04.018.

[15] Z. Vlahostergios, K. Yakinthos, A. Goulas, Separation-induced boundary layer transition: Modeling with a non-linear eddy-viscosity model coupled with the laminar kinetic energy equation, International Journal of Heat and Fluid Flow 30 (4) (2009) 617 – 636.

[16] K. Suluksna, P. Dechaumphai, E. Juntasaro, Correlations for modeling transitional boundary layers under influences of freestream turbulence and pressure gradient, International Journal of Heat and Fluid Flow 30 (1) (2009) 66 – 75.

[17] M. Bernardini, S. Pirozzoli, P. Orlandi, Compressibility effects on roughness-induced boundary layer transition, International Journal of Heat and Fluid Flow 35 (2012) 45 – 51, 7th Symposium on Turbulence & Shear Flow Phenomena (TSFP7).

[18] J. Serna, B. Lázaro, On the bursting condition for transitional separation bubbles, Aerospace Science and Technology 44 (2015) 43 – 50, instability and Control of Massively Separated Flows. doi:https://doi.org/10.1016/j.ast.2014.10.010.

[19] G. L. O. Halila, A. P. Antunes, R. G. da Silva, J. L. F. Azevedo, Effects of boundary layer transition on the aerodynamic analysis of high-lift systems, Aerospace Science and Technology 90 (2019) 233 – 245. doi:https://doi.org/10.1016/j.ast.2019.04.051.

[20] J. Xu, Z. Fu, J. Bai, Y. Zhang, Z. Duan, Y. Zhang, Study of boundary layer transition on supercritical natural laminar flow wing at high reynolds number through wind tunnel experiment, Aerospace Science and Technology 80 (2018) 221 – 231. doi:https://doi.org/10.1016/j.ast.2018.07.007.

[21] R. Vizinho, J. Morgado, J. Páscoa, M. Silvestre, Analysis of transitional flow in 3d geometries using a novel phenomenological model, Aerospace Science and Technology 45 (2015) 431 – 441. doi:https://doi.org/10.1016/j.ast.2015.06.018.

[22] S. Kubacki, E. Dick, An algebraic model for bypass transition in turbomachinery boundary layer flows, International Journal of Heat and Fluid Flow 58 (2016) 68 – 83.

[23] Q. Ye, F. F. Schrijer, F. Scarano, Geometry effect of isolated roughness on boundary layer transition investigated by tomographic piv, International Journal of Heat and Fluid Flow 61 (2016) 31 – 44, sI TSFP9 special issue.

[24] H. Medina, A. Beechook, H. Fadhila, S. Aleksandrova, S. Benjamin, A novel laminar kinetic energy model for the prediction of pretransitional velocity

fluctuations and boundary layer transition, International Journal of Heat and Fluid Flow 69 (2018) 150 – 163.

[25] J. Kiedaisch, M. Acharya, Investigation of unsteady separation over pitching airfoils at high Reynolds numbers, in: 29th AIAA, Fluid Dynamics Conference, American Institute of Aeronautics and Astronautics, Reston, Virigina, 2013. doi:10.2514/6.1998-2975.

[26] S. J. Schreck, W. E. Faller, H. E. Helin, Pitch rate and reynolds number effects on unsteady boundary-layer transition and separation, Journal of Aircraft 35 (1) (1998) 46–52.

[27] T. Lee, S. Basu, Measurement of unsteady boundary layer developed on an oscillating airfoil using multiple hot-film sensors, Experiments in Fluids 25 (2) (1998) 108–117. doi:10.1007/s003480050214.

[28] M. Tiedemann, F. Kost, Unsteady Boundary Layer Transition on a High Pressure Turbine Rotor Blade, in: Volume 3: Heat Transfer; Electric Power; Industrial and Cogeneration, ASME, 1999, p. V003T01A055. doi:10.1115/99-gt-194.

[29] T. Lee, P. Gerontakos, Investigation of flow over an oscillating airfoil, Journal of Fluid Mechanics 512 (2004) 313–341. doi:10.1017/S0022112004009851.

[30] S. Yarusevych, J. G. Kawall, P. E. Sullivan, Separated-shear-layer development on an airfoil at low reynolds numbers, AIAA Journal 46 (12) (2008) 3060–3069. doi:10.2514/1.36620.

[31] M. Masdari, M. Jahanmiri, M. R. Soltani, A. Tabrizian, M. Gorji, Experimental investigation of a supercritical airfoil boundary layer in pitching motion, Journal of Mechanical Science and Technology 31 (1) (2017) 189–196. doi:10.1007/s12206-016-1221-3.

[32] A. Tabrizian, M. Masdari, F. Ehtehadi, Frequency analysis of a supercritical airfoil boundary layer using discrete wavelet transform, in: 8th Interna-

tional Conference on Electrical, Computer, Mechanical and Mechatronics Engineering (ICE2018), Istanbul, Turkey, 2018.

[33] D. Rudmin, A. Benaissa, D. Poirel, Detection of Laminar Flow Separation and Transition on a NACA-0012 Airfoil Using Surface Hot-Films, Journal of Fluids Engineering 135 (10) (2013) 101104. doi:10.1115/1.4024807.

[34] A. Poels, D. Rudmin, A. Benaissa, D. Poirel, Localization of Flow Separation and Transition Over a Pitching NACA0012 Airfoil at Transitional Reynolds Numbers Using Hot-Films, Journal of Fluids Engineering 137 (12) (2015) 124501. doi:10.1115/1.4031008.

[35] M. Tatar, M. Tahani, M. Masdari, Numerical study of boundary layer transition using intermittency model, Aircraft Engineering and Aerospace Technology 91 (8) (2019) 1156–1168. doi:10.1108/AEAT-05-2018-0144.

[36] A. D. Gardner, K. Richter, Boundary layer transition determination for periodic and static flows using phase-averaged pressure data, Experiments in Fluids 56 (6) (2015) 119. doi:10.1007/s00348-015-1992-9.

[37] A. Goerttler, A. D. Gardner, K. Richter, Unsteady boundary layer transition detection by automated analysis of hot film data, in: Notes on Numerical Fluid Mechanics and Multidisciplinary Design, Vol. 136, Springer, Cham, 2018, pp. 387–396. doi:10.1007/978-3-319-64519-3_35.

[38] A. Grossmann, J. Morlet, Decomposition of hardy functions into square integrable wavelets of constant shape, SIAM Journal on Mathematical Analysis 15 (4) (1984) 723–736. doi:10.1137/0515056.

[39] M. Farge, Y. Guezennec, C. M. Ho, C. Meneveau, Continuous wavelet analysis of coherent structures, in: Studying Turbulence Using Numerical Simulation Databases. 3: Proceedings of the 1990 Summer Program, 1990, pp. 331–348.

[40] M. Farge, Wavelet transforms and their applications to turbulence, Annual review of fluid mechanics 24 (1) (1992) 395–458.

[41] The Path to Predicting Bypass Transition, Vol. Volume 1: Turbomachinery of Turbo Expo: Power for Land, Sea, and Air, v001T01A065. doi:10.1115/96-GT-199.

[42] S. W. M. Lang, U. Rist, Investigations on disturbance amplification in a laminar separation bubble by means of lda and piv, 11th International Symposium on Laser Techniques to Fluid Mechanics, 2002, pp. 331–348.

[43] U. Rist, On instabilities and transition in laminar separation bubbles, in: Proc. CEAS Aerospace Aerodynamics Research Conference, 2002, pp. 10–12.

[44] H. Nobach, C. Tropea, L. Cordier, J.-P. Bonnet, J. Delville, J. Lewalle, M. Farge, K. Schneider, R. Adrian, Review of Some Fundamentals of Data Processing, Springer Berlin Heidelberg, Berlin, Heidelberg, 2007, pp. 1337–1398. doi:10.1007/978-3-540-30299-5_22.

[45] C. Torrence, G. P. Compo, A Practical Guide to Wavelet Analysis., Bulletin of the American Meteorological Society 79 (1) (1998) 61–78.